ELSEVIER

CrossMark

The Spine Journal 15 (2015) 992–999

THE SPINE JOURNAL

Basic Science

Validation of cone-beam computed tomography and magnetic resonance imaging of the porcine spine: a comparative study with multidetector computed tomography and anatomical specimens

Ricardo Miguel Costa de Freitas, MD[a,b,*], Celi Santos Andrade, PhD[a], José Guilherme Mendes Pereira Caldas, PhD[a], Alexandre Fligelman Kanas, MD[a], Richard Halti Cabral, PhD[c], Miriam Harumi Tsunemi, PhD[d], Hernán Joel Cervantes Rodríguez, PhD[e], Said Rahnamaye Rabbani, PhD[e]

[a]*Radiology Department, Instituto de Radiologia-InRad, Faculdade de Medicina da Universidade de São Paulo, Av. Dr. Enéas de Carvalho Aguiar, s/n° - Rua 1 - Cerqueira César, CEP: 05403-900, São Paulo, SP, Brazil*

[b]*Radiology Unit, Instituto do Câncer do Estado de São Paulo-ICESP, Avenida Doutor Arnaldo, 251, Cerqueira César, 01246-000, São Paulo, SP, Brazil*

[c]*Anatomy Department, University of São Paulo Institute of Biomedical Sciences, Av. Prof. Lineu Prestes, 2415 - Cidade Universitária, Butantã, 05508-900, São Paulo, SP, Brazil*

[d]*Biostatistics Department, Universidade Estadual Paulista Júlio de Mesquita Filho Biosciences Institute, Dist. Rubião Jr, 18618-970, Botucatu, SP, Brazil*

[e]*Magnetic Resonance Imaging Laboratory, Instituto de Física da Universidade de São Paulo, Rua do Matão, Travessa R, 187, Cidade Universitária, 05508-090, São Paulo, Brazil*

Received 22 January 2014; revised 10 October 2014; accepted 8 January 2015

Abstract

BACKGROUND CONTEXT: New spinal interventions or implants have been tested on ex vivo or in vivo porcine spines, as they are readily available and have been accepted as a comparable model to human cadaver spines. Imaging-guided interventional procedures of the spine are mostly based on fluoroscopy or, still, on multidetector computed tomography (MDCT). Cone-beam computed tomography (CBCT) and magnetic resonance imaging (MRI) are also available methods to guide interventional procedures. Although some MDCT data from porcine spines are available in the literature, validation of the measurements on CBCT and MRI is lacking.

PURPOSE: To describe and compare the anatomical measurements accomplished with MDCT, CBCT, and MRI of lumbar porcine spines to determine if CBCT and MRI are also useful methods for experimental studies.

STUDY DESIGN: An experimental descriptive-comparative study.

METHODS: Sixteen anatomical measurements of an individual vertebra from six lumbar porcine spines (n=36 vertebrae) were compared with their MDCT, CBCT, and MRI equivalents. Comparisons were made for the absolute values of the parameters.

RESULTS: Similarities were found in all imaging methods. Significant correlation ($p<.05$) was observed with all variables except those that included cartilaginous tissue from the end plates when the anatomical study was compared with the imaging methods.

CONCLUSIONS: The CBCT and MRI provided imaging measurements of the lumbar porcine spines that were similar to the anatomical and MDCT data, and they can be useful for specific experimental research studies.

Keywords: Anatomy; Porcine; Lumbar spine; Cone-beam computed tomography; Multidetector computed tomography; Magnetic resonance imaging

FDA device/drug status: Not applicable.

Author disclosures: ***RMCF:*** Grant: FAPESP Government agency (No. 2011/51222-8) (B, Paid directly to institution). ***CSA:*** FAPESP Government agency (2012/00398-1) (B, Paid directly to institution). ***JGMPC:*** FAPESP Government agency (No. 2011/51222-8) (B, Paid directly to institution). ***AFK:*** Nothing to disclose. ***RHC:*** Nothing to disclose. ***MHT:*** Nothing to disclose. ***HJCR:*** Nothing to disclose. ***SRR:*** Nothing to disclose.

The disclosure key can be found on the Table of Contents and at www.TheSpineJournalOnline.com.

This study was supported by government research grant and the authors disclose no conflict of interest.

* Corresponding author. Radiology Unit, Instituto do Câncer do Estado de São Paulo, Avenida Doutor Arnaldo, 251-Cerqueira César, São Paulo 01246-000, SP, Brazil. Tel.: (55) 113893-2945.

E-mail address: ricardomcfreitas@gmail.com (R.M.Costade Freitas)

http://dx.doi.org/10.1016/j.spinee.2015.01.017

Introduction

Experiments in animals have been performed as a model to preclinical essays to test the safety of new techniques or devices in surgical or interventional image-guided methods before they are carried out in humans. The more appropriate models comparable with human spine samples are obtained from porcine or canine spines [1]. Porcine spines are easily available, and spinal interventions or implants have been tested on ex vivo or in vivo swine models [2–4].

A database of anatomical measurements of porcine spines is important to provide anatomical references when developing such implants or techniques. Comparisons among porcine spine anatomy and other animal models or between human and swine spines have been previously described [5–7].

Interventional procedures of the spine are mostly guided by fluoroscopy in clinical practice. Moreover, these procedures can also be carried out with multidetector computed tomography (MDCT), particularly when high precision is crucial for more difficult or complex cases [8]. Cone-beam computed tomography (CBCT) and magnetic resonance imaging (MRI) are also available to guide interventional spine procedures [9,10]. In the experimental spinal research field, high precision images may also be essential in the development and evaluation of new techniques or devices, such as disc punctures, lumbar interbody fusion, or tumor ablation [11–15].

Although some MDCT data from porcine spines are described in the literature [5], its comparison with CBCT or MRI is lacking. The aim of this descriptive study was to compare the anatomical and MDCT dimensions of the individual vertebrae from six lumbar porcine spines with their CBCT and MRI measurements to determine if the last two methods are also useful in porcine spine experimental studies.

Materials and methods

This work was approved by our institutional Animal Use and Care Committee (registry number: 239/11). Six fresh skeletally immature spines from healthy 3- to 4-month-old farm bred domestic Landrace pigs (*Sus scrofa domesticus*) with average weight of 35 kg (range 32–38 kg) were obtained from cadavers. These swines were euthanized after abdominal surgery at the Experimental Surgery Laboratory of our institution, following the ethics and management welfare criteria applied to the experimental animals [16].

All spines were dissected from L1–L6 and only paravertebral musculature was initially removed. The specimens were then kept in formalin and imaging was obtained (Fig. 1).

Multidetector computed tomography scans (GE Dual Energy 64-slices Discovery CT; GE Healthcare, Waukesha, WI, USA) were obtained with a slice thickness (ST) of 0.625 mm and a reformatted resolution of 0.35±0.05 mm protocol.

Cone-beam computed tomography scans (GE Innova 4100; GE Healthcare, Inc., Waukesha, WI, USA) were performed with the following protocol: fluoroscopy frame rate: 30 images/s; filter: 0.2 mmCU; 87 kV; and 0.5 mA.

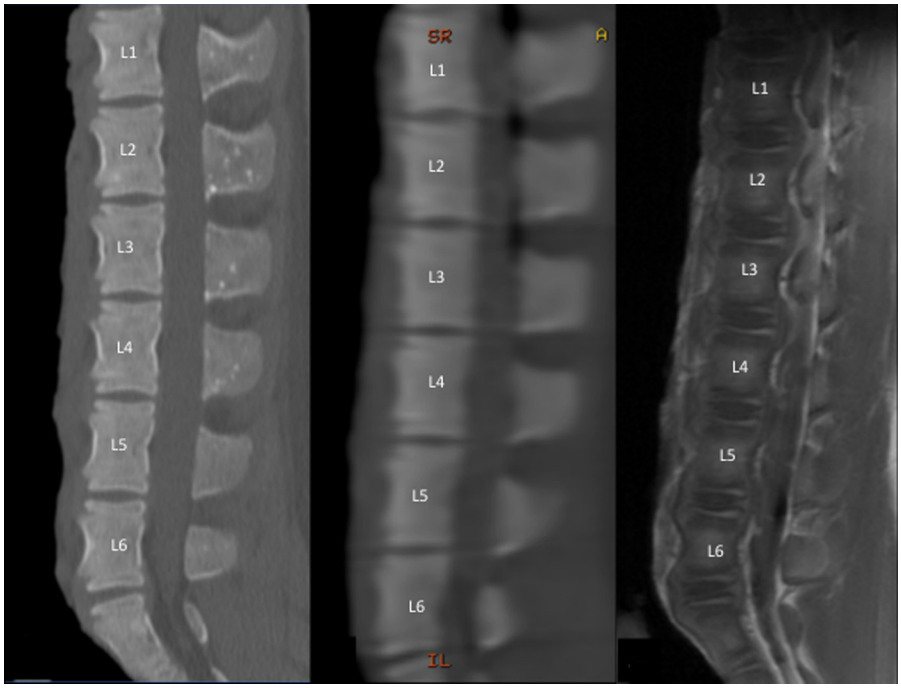

Fig. 1. Sagittal views from lumbar porcine spine imaging: (Left) multidetector computed tomography, (Middle) cone-beam computed tomography, and (Right) T1-weighted magnetic resonance imaging. Lumbar vertebral levels were indicated from L1–L6. After imaging acquisition, the vertebrae were dissected for anatomical study.

Table 1
Measured parameters and abbreviations of the porcine vertebrae

Parameter	Abbreviation
Anterior vertebral body height	AVBh
Central vertebral body height	CVBh
Posterior vertebral body height	PVBh
Upper end plate width	UEw
Upper end plate depth	UEd
Lower end plate width	Lew
Lower end plate depth	Led
Vertebral disc height	VDh
Spinal canal width	SCw
Spinal canal depth	SCd
Transverse process length	TPl
Spinous process length	SPl
Averaged pedicle width	Pw (R+L/2)
Averaged pedicle height	Ph (R+L/2)

R, right; L, left.

Three-dimensional (3D) computed tomography (CT) was acquired with a rotation speed of 20°/s; source-to-image receptor distance: 1,195 mm; 0.3 mmCU; 85 kV; 62.8 mA; and 7 milliseconds.

Magnetic resonance imaging was obtained from a 1.5 Tesla Phillips Gyroscan S15/HP ACSII (Phillips Medical Systems, Best, The Netherlands). T1- and T2-weighed spin-echo sequences were obtained as follows: axial series with echo number (EN): 1; slice factor (SF): 1; slice number (SN): 16 to 18; ST: 5 mm; number of signals averaged (NSA): 8; field of view (FOV): 10 cm; time of repetition (TR): 34 and 3,199 milliseconds; time of echo (TE): 21 and 178 milliseconds (T1 and T2, respectively); sagittal series with EN: 1; SF: 1; SN: 18; thickness: 4 mm; NSA: 8; FOV: 20 cm; TR: 535 and 1,665 milliseconds; TE: 12 and 120 milliseconds (T1 and T2, respectively); coronal views with EN: 1; SF: 1; SN: 8; thickness: 5 mm; NSA: 8; FOV: 20 cm; TR: 450 and 1,665 milliseconds (T1 and T2, respectively); TE: 19 and 120 milliseconds (T1 and T2, respectively).

Two experienced radiologists (RMCF and CSA) measured independently 16 anatomical dimensions (Table 1, Fig. 2) per vertebra from the two-dimensional views with a multiplanar viewer. The measurements from MRI were obtained with the scanner interface—Phillips Dicom Viewer; Phillips Medical Systems, The Netherlands. Measurements from the MDCT were acquired with the same software interface used for MRI. On the other hand, CBCT measurements were made with its own interface (Innova 3DXR 1.0; GE Healthcare, Inc., USA). Multiplanar reconstructions from 3D datasets (MDCT and CBCT) were used to select the optimum measurement planes according to the specific measurements. The pedicle width and height were averaged from the left and right pedicle measurements.

After imaging acquisition, spinal segments were prepared for dissection with the help of a pressure cooker for 30 minutes. The vertebrae were then harvested with sharp dissection. Fifteen anatomical parameters (Table 1, Fig. 2) from each vertebra were recorded by three independent observers (RMCF, AFK, RHC) with the aid of a digital vernier caliper

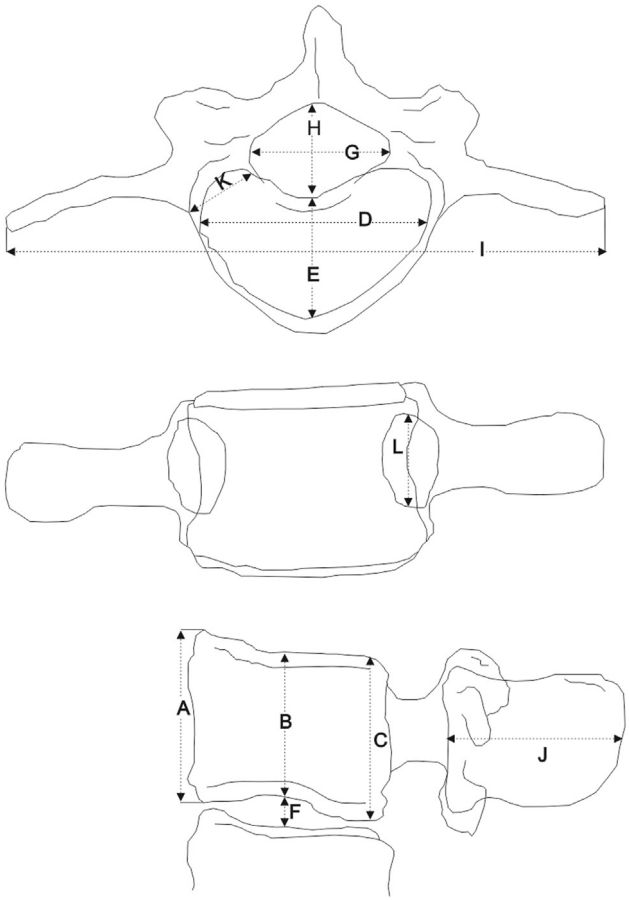

Fig. 2. Anatomical parameters: (A) anterior, (B) central, and (C) posterior vertebral body height; (D) upper and lower end plate width; (E) upper and lower end plate depth; (F) vertebral disc height*; (G) spinal canal width; (H) spinal canal depth; (I) transverse process length; (J) spinous process length; (K) averaged pedicle width; (L) averaged pedicle height. *Measured only on imaging examinations.

(Mitutoyo CD-6 CSX; Tokyo, Japan; accuracy ±0.02 mm). Each measurement was recorded three times by each observer in the anatomical study (AS).

The mean, standard deviation (SD), and 95% confidence interval were computed using Microsoft Excel (Excel 2010, Microsoft Corporation, Redmont, WA, USA). An average of the readings by all the observers per parameter was subsequently calculated. The interclass correlation coefficient, the intraobserver agreement, and the Spearman correlation tests of the MDCT, CBCT, MRI, and anatomical dimensions were calculated. A multivariable analysis was performed to confirm if data from all readers could be combined. Bland-Altman analyses were also performed for each parameter, technique, reader, and animal. As a large amount of results were generated, the coefficient of variation was then applied for each technique to estimate the variation of measurements in relation to the mean and to the maximum values of the SDs. All tests were performed by a statistical expert with the software SPSS (Statistical Package for the Social Sciences, version 17.0 Release 17.0.1, IBM Corporation, Armonk, NY, USA).

Table 2
Descriptive statistics of anatomical and imaging measurements of porcine spine

Parameters	Modality	N	Mean (mm)	SD (mm)	Parameter	Modality	N	Mean (mm)	SD (mm)
AVBh	AS	36	19.24	1.16	VDh	AS	—	—	—
	CBCT	36	20.71	1.21		CBCT	36	2.91	0.46
	MRI	36	19.91	1.14		MRI	36	3.65	0.42
	MDCT	36	20.83	1.19		MDCT	36	3.24	0.52
CVBh	AS	36	17.16	1.17	SCw	AS	36	14.13	2.29
	CBCT	36	19.46	1.21		CBCT	36	13.47	2.31
	MRI	36	17.57	1.06		MRI	36	15.28	2.56
	MDCT	36	19.10	1.19		MDCT	36	14.47	2.45
PVBh	AS	36	19.38	1.43	SCd	AS	36	8.68	0.69
	CBCT	36	20.31	1.33		CBCT	36	8.64	0.76
	MRI	36	20.68	1.72		MRI	36	10.19	1.29
	MDCT	36	20.98	1.38		MDCT	36	8.83	0.61
UEw	AS	36	23.06	1.72	TPl	AS	36	61.49	8.02
	CBCT	36	24.28	2.02		CBCT	36	68.01	8.28
	MRI	36	26.43*	2.32		MRI	36	66.15	11.06
	MDCT	36	24.25*	1.81		MDCT	36	66.93	7.85
UEd	AS	36	12.21	0.90	SPl	AS	36	11.33	2.05
	CBCT	36	12.87	0.82		CBCT	36	13.81	2.26
	MRI	36	15.44	1.48		MRI	36	13.49	2.26
	MDCT	36	12.90	0.81		MDCT	36	13.34	2.26
LEw	AS	36	23.71	1.60	Pw	AS	36	11.13	1.18
	CBCT	36	24.85	1.97		CBCT	36	11.44	1.23
	MRI	35	26.64*	2.46		MRI	36	10.55	1.20
	MDCT	36	25.02	1.70		MDCT	36	10.27	1.23
LEd	AS	36	11.87	0.71	Ph	AS	36	7.82	0.52
	CBCT	36	12.65	0.69		CBCT	36	8.53	0.51
	MRI	36	14.53	1.07		MRI	36	7.37	0.68
	MDCT	36	12.02	0.83		MDCT	36	7.72	0.56

SD, standard deviation; AVBh, anterior vertebral body height; PVBh, posterior vertebral body height; CVBh, central vertebral body height; UEw, upper end plate width; UEd, upper end plate depth; LEw, lower end plate width; LEd, lower end plate depth; VDh, vertebral disc height; SCw, spinal canal width; SCd, spinal canal depth; TPl, transverse process length; SPl, spinous process length; Pw, averaged pedicle width; Ph, averaged pedicle height; AS, anatomical study; CBCT, cone-beam computed tomography; MRI, magnetic resonance imaging; MDCT, multidetector computed tomography.

* Significant p values were found when compared with AS.

Results

This study generated 8,316 entries (AS=4,860 entries; CBCT, MDCT, and MRI=1,152 entries each). The anatomical dimensions and imaging data were summarized in Table 2. The intraclass correlations of each parameter and method were summarized in Table 3. The interclass correlations between the AS and MDCT, CBCT, or MRI data were evaluated with the Spearman correlation coefficient (Table 4).

There was significant positive correlation ($p<.05$) for the anatomical dimensions of the spinal canal width and depth, transverse process length, and spinous process length among all imaging methods and for the anatomical dimensions of the averaged pedicle width and height among CBCT and MDCT imaging. No statistic correlation was observed between the AS and the imaging data for the following parameters encompassing the end plates: anterior vertebral body height, central vertebral body height, posterior vertebral body height, upper end plate width, upper end plate depth, lower end plate width, lower end plate depth, and the averaged pedicle width and height measured at MRI series.

The multivariable analysis showed a significant effect of the reader in only one parameter (anterior vertebral body height, at CBCT imaging), taking into account the mean of each technique as the dependent variable and the reader as the independent variable. In all the other 51 analyses (13 parameters vs. 4 techniques), no significant differences were observed between the readers. The Pearson correlation coefficient of the pooled data also detected a positive significant correlation among the imaging techniques and the AS in most of the parameters evaluated.

Bland-Altman analyses indicated that the mean and SD of the coefficient of variation among all the parameters and vertebrae were about 7 ± 2 mm. The average differences between the readers were approximately 0.05 mm, whereas the highest SD evaluated was 5 mm (MRI technique). The most precise technique was the AS, with an average difference of 0.05 mm and a mean SD of 0.151 mm (Table 5).

Discussion

The three imaging modalities evaluated (CBCT, MDCT, and MRI) in this study showed good correlation with each other as demonstrated with the Spearman correlation coefficients (r), and also when compared with the AS dimensions (Table 4). The Bland-Altman limits of agreement

Table 3
Intraclass correlation of parameters obtained from imaging data (MDCT, CBCT, and MRI) and AS

Parameter	CBCT	95% CI	MRI	95% CI	MDCT	95% CI	AS	95% CI
AVBh	0.902	0.817–0.949	0.754	0.568–0.866	0.949	0.903–0.974	0.993	0.987–0.996
CVBh	0.934	0.875–0.966	0.899	0.811–0.947	0.876	0.770–0.935	0.997	0.993–0.998
PVBh	0.943	0.892–0.971	0.966	0.934–0.982	0.974	0.950–0.987	0.991	0.983–0.996
UEw	0.929	0.866–0.963	0.920	0.849–0.959	0.967	0.937–0.983	0.998	0.996–0.999
UEd	0.896	0.805–0.945	0.981	0.963–0.990	0.887	0.789–0.941	0.986	0.973–0.993
LEw	0.917	0.843–0.957	0.930	0.866–0.964	0.967	0.936–0.983	0.996	0.992–0.998
LEd	0.872	0.764–0.933	0.914	0.838–0.955	0.853	0.730–0.922	0.978	0.958–0.989
VDh	0.857	0.738–0.925	0.952	0.907–0.975	0.882	0.781–0.938	—	—
SCw	0.985	0.970–0.992	0.989	0.979–0.995	0.979	0.959–0.989	0.999	0.999–1.000
SCd	0.836	0.701–0.913	0.945	0.894–0.971	0.861	0.744–0.926	0.979	0.959–0.989
TPl	0.995	0.989–0.997	0.969	0.940–0.984	0.995	0.989–0.997	1.000	0.999–1.000
SPl	0.976	0.954–0.988	0.995	0.991–0.998	0.978	0.957–0.989	0.993	0.987–0.997
Pw	0.915	0.840–0.956	0.951	0.906–0.975	0.930	0.868–0.964	0.995	0.991–0.998
Ph	0.858	0.740–0.925	0.854	0.733–0.923	0.908	0.828–0.952	0.955	0.914–0.977

CI, confidence interval; AVBh, anterior vertebral body height; PVBh, posterior vertebral body height; CVBh, central vertebral body height; UEw, upper end plate width; UEd, upper end plate depth; LEw, lower end plate width; LEd, lower end plate depth; VDh, vertebral disc height; SCw, spinal canal width; SCd, spinal canal depth; TPl, transverse process length; SPl, spinous process length; Pw, averaged pedicle width; Ph, averaged pedicle height; AS, anatomical study; CBCT, cone-beam computed tomography; MRI, magnetic resonance imaging; MDCT, multidetector computed tomography.

analyses revealed little difference between readers (Table 5), whereas multivariate analyses indicated that data from all readers could be combined. The differences observed when AS data were matched to the imaging data measurements could be attributed to the presence of the cartilaginous tissue of the growth end plates. As this study was carried out in young porcine spines, the end plates were not mature. A considerable amount of cartilaginous tissue was included in the imaging measurements, because it was collected before harvesting the vertebrae from soft tissue. On the other hand, the AS was performed after harvesting the vertebrae. This fact could easily explain the lower mean values measured with the digital caliper at the AS when compared with the measurements of the imaging data (CBCT, MDCT, and MRI).

Dath et al. (2007) [6] performed an anatomical comparison between the porcine lumbar spine and the human spine. They evaluated porcine spines obtained from animals aged 18 to 24 months old and weighing 60 to 80 kg as they considered that the porcine spines at that age could be better comparable with human adult spines. In contrast, our study was carried out in a younger skeletally immature sample of animals. In fact, the epiphyses of the long bones are not completely closed in domestic swine until approximately 3.5 years [17]. Differences in bone composition or in biomechanical properties related to age (young×adult swine) were not the scope of this study.

Anatomical structures of young individuals such as the growth end plates must be taken into account when performing spinal research in younger pigs. For example, when the experimental work includes spine fusion, some pig species, such as the Göttingen minipig, are better suitable as their growth plate closure usually happens before 2 years [17]. Instead, if the experiment results are not influenced by the presence or absence of the growth end plates, it may be economically advantageous to include young animals in a protocol of experimental research.

Busscher et al. (2010) [5] compared MDCT data from young porcine spines (4 months old) and older human spines (55 to 84 years old), and they also observed good agreement of the intra- and interclass correlations. The parameters were assessed only with MDCT, which has the highest level of resolution as an imaging method to depict cortical bone structures when compared with CBCT or MRI. In our study, we included the CBCT and MRI data to compare with MDCT and the AS, adding some valuable information regarding the usefulness of the former two imaging methods. Our MRI data were acquired after embalming the spines in formalin. The degradation effect of the formalin fixation on the MRIs did not significantly affect the interpretation of gross anatomical musculoskeletal structures, including bone and cartilage [18,19].

Pedicle height and width reached no statistic correlation in MRI measurements and the AS. To explain this difference, we hypothesized that when these two small parameters were measured at coronal views of MDCT or CBCT reformatted images at the workstations, the cortical bone was taken into account, but the same structure could not be easily depicted in MRI in comparison with the other two imaging methods. Probably, the cortical bone was not completely included in the MRI measurements. Moreover, the MRI series were not volumetric, and so slight distortions related to positioning of the specimens in the scanner could not be corrected, as opposed to MDCT or CBCT.

Although CBCT has been developed in the last 20 years, it has just recently been incorporated in the interventional radiology practice [9,20]. It uses state-of-the-art C-arm flat-panel fluoroscopy systems to generate X-ray images and acquire and display 3D images. The flat-panel offers

Table 4
ICC between measured parameters and imaging data (CBCT, MDCT, and MRI), and Spearman correlation coefficients (r) among the average values from the imaging data (MDCT, CBCT, and MRI) and the AS

			95% CI		Spearman correlation test			
Parameter	Procedure	ICC	LL	SL		CBCT	MRI	MDCT
AVBh	CBCT	−1.285	−3.452	−0.169	R	−0.211	−0.167	−0.188
	MRI	−0.391	−1.709	0.289	p	.217	.331	.273
	MDCT	−1.573	−4.013	−0.316	N	36	36	36
	Global	0.466	0.113	0.702				
CVBh	CBCT	−1.795	−4.445	−0.430	R	−0.026	−0.082	−0.056
	MRI	−0.212	−1.362	0.380	p	.880	.634	.747
	MDCT	−1.330	−3.540	−0.192	N	36	36	36
	Global	0.347	−0.085	0.636				
PVBh	CBCT	0.089	−0.775	0.534	R	0.168	0.152	0.122
	MRI	0.079	−0.794	0.529	p	.326	.376	.480
	MDCT	−0.496	−1.916	0.235	N	36	36	36
	Global	0.705	0.509	0.835				
UEw	CBCT	0.188	−0.582	0.585	R	0.269	0.430	0.332
	MRI	−0.355	−1.641	0.307	p	.113	**.009**	**.048**
	MDCT	0.264	−0.435	0.623	N	36	36	36
	Global	0.669	0.450	0.815				
UEd	CBCT	−0.116	−1.175	0.429	R	0.050	0.145	0.156
	MRI	−3.014	−6.821	−1.053	p	.770	.399	.364
	MDCT	0.027	−0.896	0.502	N	36	36	36
	Global	−0.292	−1.147	0.280				
LEw	CBCT	0.201	−0.557	0.591	R	0.200	0.384	0.306
	MRI	−0.208	−1.377	0.388	p	.242	**.023**	.069
	MDCT	0.276	−0.411	0.629	N	36	35	36
	Global	0.594	0.320	0.776				
LEd	CBCT	−0.337	−1.605	0.316	R	0.041	−0.123	0.156
	MRI	−4.082	−8.902	−1.600	p	.810	.477	.363
	MDCT	0.339	−0.288	0.662	N	36	36	36
	Global	−0.868	−2.105	−0.042				
SCw	CBCT	0.840	0.689	0.918	R	0.739	0.836	0.789
	MRI	0.837	0.683	0.917	p	**<.001**	**<.001**	**<.001**
	MDCT	0.881	0.767	0.939	N	36	36	36
	Global	0.940	0.901	0.967				
SCd	CBCT	0.758	0.529	0.876	R	0.502	0.578	0.640
	MRI	−0.129	−1.200	0.422	p	**.002**	**<.001**	**<.001**
	MDCT	0.849	0.706	0.923	N	36	36	36
	Global	0.517	0.198	0.731				
TPl	CBCT	0.683	0.382	0.838	R	0.745	0.646	0.749
	MRI	0.700	0.416	0.847	p	**<.001**	**<.001**	**<.001**
	MDCT	0.738	0.490	0.866	N	36	36	36
	Global	0.891	0.819	0.939				
SPl	CBCT	0.587	0.196	0.789	R	0.867	0.757	0.893
	MRI	0.578	0.178	0.784	p	**<.001**	**<.001**	**<.001**
	MDCT	0.723	0.460	0.858	N	36	36	36
	Global	0.895	0.825	0.941				
Ph	CBCT	0.812	0.633	0.904	R	0.701	0.329	0.565
	MRI	0.513	0.051	0.751	p	**<.001**	0.050	**<.001**
	MDCT	0.692	0.399	0.842	N	36	36	36
	Global	0.741	0.569	0.855				
Pw	CBCT	−0.151	−1.243	0.411	R	0.431	0.319	0.729
	MRI	0.087	−0.779	0.533	p	**.009**	0.058	**<.001**
	MDCT	0.757	0.527	0.876	N	36	36	36
	Global	0.534	0.226	0.740				

ICC, interclass correlation; AS, anatomical study; CBCT, cone-beam computed tomography; MRI, magnetic resonance imaging; MDCT, multidetector computed tomography; LL, lower limit; SL, superior limit; CI, confidence interval; AVBh, anterior vertebral body height; PVBh, posterior vertebral body height; CVBh, central vertebral body height; UEw, upper end plate width; UEd, upper end plate depth; LEw, lower end plate width; LEd, lower end plate depth; SCw, spinal canal width; SCd, spinal canal depth; TPl, transverse process length; SPl, spinous process length; Pw, averaged pedicle width; Ph, averaged pedicle height.

Note: Significant p values are printed in bold type.

Table 5
CV from Bland-Altman limits of agreement analysis, applied for each technique, and the variation of measurements in relation to the mean and maximum values of the SDs

	CV		Differences between readers		
Technique	Mean	SD	Mean	SD (mean)	SD (max)
CBCT	7.31	1.67	0.10	0.416	1.256
MDCT	7.69	2.66	0.03	0.405	1.054
MRI	8.81	2.16	0.10	0.517	5.184
AS	6.45	0.75	0.05	0.151	0.327

CV, coefficient of variation (millimeter); SD, standard deviation; SD (max), maximum values of SD; AS, anatomical study; CBCT, cone-beam computed tomography; MRI, magnetic resonance imaging; MDCT, multidetector computed tomography.

Note: All measurements are provided in millimeter.

higher spatial resolution than the conventional image intensifier detector systems, and the evolution of this technology provides CT-like images in multiple viewing planes. Its applicability is expanded to vascular interventional radiology and nonvascular interventional procedures.

Spine interventions are usually performed with fluoroscopic guidance alone, which provides sufficient information to guide appropriate needle placement, for example, to guide the injection of acrylic cement in lower thoracic or lumbar spine interventions. However, for difficult spine procedures, CBCT or MDCT show in more detail the safer regions suitable for needle placement and depict the exact needle locations in 3D in comparison with fluoroscopy. Cone-beam computed tomography is optimal when real-time fluoroscopic imaging and CT-like imaging are useful and complementary for complex percutaneous interventions or high-risk procedures [9].

Magnetic resonance imaging-guided interventions have been applied in the research and clinical fields to guide biopsies and therapies in the last 20 years. Its limitations still include high costs of implementation (MRI equipment and MRI-compatible instruments and devices), but there is an increasing acceptance of its applicability in clinical practice [21].

Conclusions

Despite the small dimensions of the evaluated spine structures, CBCT, MDCT, and MRI are comparable imaging methods in most of the evaluated parameters, whereas multivariable analysis showed no significant differences between the readers. These imaging techniques can be useful when studying porcine spines in experimental models. Nevertheless, MRI has some specific characteristics that might be taken into account when spinal anatomical comparisons are performed, especially in immature specimens with growing cartilaginous end plates. The anatomical evaluation of porcine spines with CBCT and MRI of the present study provides a radiologic database to promote the development of new technologies in spinal research.

Acknowledgments

Financial support was provided by São Paulo Research Foundation - FAPESP (R.M.C.F, J.G.M.P.C, 2011/51222-8). Scholarships were provided by FAPESP (C.S.A., 2012/00398-1).

References

[1] Aerssens J, Boonen S, Lowet G, Dequeker J. Interspecies differences in bone composition, density and quality: potential implications for *in vivo* bone research. Endocrinology 1998;139:663–70.
[2] Christensen FB, Dalstra M, Sejling F, Overgaard S, Bunger C. Titanium-alloy enhances bone-pedicle screw fixation: mechanical and histomorphometrical results of titanium-alloy versus stainless steel. Eur Spine J 2000;9:97–103.
[3] Cunningham BW, Lewis SJ, Long J, Dmtriev AE, Linville DA, Bridwell KH. Biomechanical evaluation of lumbosacral reconstruction techniques for spondylolisthesis: an in vitro porcine model. Spine 2002;27:2321–7.
[4] Yazici M, Pekmezci M, Cil A, Alanay A, Acaroglu E, Oner FC. The effect of pedicle expansion on pedicle morphology and biomechanical stability in the immature porcine spine. Spine 2006;31:E826–9.
[5] Busscher I, Ploegmakers JJ, Verkerke GJ, Veldhuizen AG. Comparative anatomical dimensions of the complete human and porcine spine. Eur Spine J 2010;19:1104–14.
[6] Dath R, Ebinesan AD, Porter KM, Miles AW. Anatomical measurements of porcine lumbar vertebrae. Clin Biomech 2007;22:607–13.
[7] Sheng SR, Wang XY, Xu HZ, Zhu GQ, Zhou YF. Anatomy of large animal spines and its comparison to the human spine: a systematic review. Eur Spine J 2010;19:46–56.
[8] Gangi A, Dietemann JL, Mortazavi R, Pfleger D, Kauff C, Roy C. CT-guided interventional procedures for pain management in the lumbosacral spine. Radiographics 1998;18:621–33.
[9] Wallace MJ, Kuo MD, Glaiberman C, Binkert CA, Orth RC, Soulez G. Three-dimensional c-arm cone-beam CT: applications in the interventional suite. J Vasc Interv Radiol 2008;19:799–813.
[10] Tuncalli K, Morrison PR, Winalski CS, Carrino JA, Shankar S, Ready JE, et al. MRI-guided percutaneous cryotherapy for soft-tissue and bone metastases: initial experience. AJR Am J Roentgenol 2007;189:232–9.
[11] Nour SG, Aschoff AJ, Mitchell ICS, Emancipator SN, Duerk JL, Lewin JS. MR imaging-guided radio-frequency thermal ablation of the lumbar vertebrae in porcine models. Radiology 2002;224:452–62.
[12] Mahar AT, Bagheri R, Oka R, Kostial P, Akbarnia BA. Biomechanical comparison of different anchors (foundations) for the pediatric dual growing rod technique. Spine J 2008;8:933–9.
[13] Abbah SA, Lam CXL, Hutmacher DW, Goh JCH, Wong HK. Biological performance of a polycaprolactone-based scaffold used as fusion cage device in a large animal model of spinal reconstructive surgery. Biomaterials 2009;30:5086–93.
[14] Iatridis JC, Nicoll SB, Michalek AJ, Walter BA, Gupta MS. Role of biomechanics in intervertebral disc degeneration and regenerative therapies: what needs repairing in the disc and what are promising biomaterials for its repair? Spine J 2013;13:243–62.
[15] Pezeshki PS, Woo J, Akens MK, Davies JE, Gofeld M, Whyne CM, et al. Evaluation of a bipolar-cooled radiofrequency device for ablation of bone metastases: preclinical assessment in porcine vertebrae. Spine J 2014;14:361–70.
[16] Damy SB, Camargo RS, Chammas R, Poli-de-Figueiredo LF. The fundamentals of experiments with animals—applications in experimental surgery. Rev Assoc Med Bras 2010;56:103–11.
[17] Swindle M. Musculoskeletal system and orthopedic procedures. In: Swindle M, ed. Swine in the laboratory: surgery, anesthesia, imaging and experimental techniques. Boca Raton: CRC Press, 2007:293–8.

[18] Entius CAC, van Rijn RR, Zwamborn AW, Kleinrensink GJ, Robben SGF. Influence of formaldehyde/phenol fixation on MRI of the stifle joint and correlation with plastinated slices. J Int Soc Plastination 2004;19:26–32.

[19] Van der Made AD, Maas M, Beenen LF, Oostra RJ, Kerkhoffs GM. Postmortem imaging exposed: an aid in MR imaging of musculoskeletal structures. Skeletal Radiol 2013;42:467–72.

[20] Pedicelli A, Verdolotti T, Pompucci A, Desiderio F, D'Argento F, Colosimo C, et al. Interventional spinal procedures guided and controlled by a 3D rotational angiographic unit. Skeletal Radiol 2011;40:1595–601.

[21] Mortele KJ, Tuncali K, Cantisani V, Shankar S, vanSonnenberg E, Tempany C, et al. MRI-guided abdominal intervention. Abdom Imaging 2003;28:756–74.